Angle-resolved photoemission study of half-monolayer O and S structures on the Rh(100) surface

J. R. Mercer, P. Finetti, M. J. Scantlebury, U. Beierlein,* V. R. Dhanak, and R. McGrath†
IRC in Surface Science, The University of Liverpool, P.O. Box 147, Liverpool L69 3BX, United Kingdom
(Received 25 October 1996; revised manuscript received 2 December 1996)

The valence-band photoemission of the Rh(100)-$c(2\times2)$-O, Rh(100)-$(2\times2)p4g$-O, and Rh(100)-$c(2\times2)$-S surfaces has been investigated using an incident photon energy of 38 eV, along both the $\Gamma X'$ and $\Gamma M'$ directions. Local density of states calculations have also been performed for the $c(2\times2)$-O and $c(2\times2)$-S phases using density-functional theory. For each surface overlayer the angle-resolved photoemission measurements show significant differences in the dispersion of features with binding energies between 3 and 6 eV. These peaks are assigned with reference to the density of states calculations, and the origins of the differences in dispersion are discussed in relation to the different geometric structures. [S0163-1829(97)09415-0]

I. INTRODUCTION

The study of adsorbates on transition-metal surfaces has been the subject of a large number of investigations, due primarily to the technological application of transition metals as catalysts. Two extensively studied adsorbates on transition metals are oxygen and sulphur, the former being a catalytic promoter[1] while the latter is well known as a catalytic poison.[2] On the Rh(100) surface although both O atoms and S atoms sit in fourfold hollow sites at saturation coverage,[3,4] only the O atoms cause the substrate surface layer to reconstruct.[3] If the fundamentals of O and S adsorption on Rh(100) are to be fully understood, a vital step is to determine the electronic structure. It is with this motivation that we present an angle-resolved photoemission study of O and S adsorption on the Rh(100) surface. Our aim is to extend the electronic structure database for adatoms on fcc metal surfaces and to compare the reconstructed and unreconstructed surfaces for any significant trends.

The O on Rh(100) system has been previously investigated using low-energy electron diffraction (LEED),[3,5–10] scanning tunneling microscopy (STM),[3] and core-level photoemission.[11] The latter study also includes some angle-resolved photoemission along the $\langle 100\rangle$ principal azimuth only.[11]

The spot profile analysis low-energy electron diffraction (SPA-LEED) and STM study[3] showed that O can be reliably dosed on the Rh(100) surface to produce distinct $p(2\times2)$ and $c(2\times2)$ phases at local coverages of 1/4 and 1/2 monolayer (ML), respectively. Further dosing of the $c(2\times2)$ phase with oxygen gives rise to a $p(2\times2)$ LEED pattern that at normal incidence shows systematic absences of the $(n+\frac{1}{2},0)$ and $(0,m+\frac{1}{2})$ spots, STM images of this phase show the symmetry is $(2\times2)p4g$ rather than $(2\times2)pgg$ as had been previously suggested by a LEED structural study.[9] This $(2\times2)p4g$ structure can be adequately described by the ''clock'' reconstruction models existing for the $(2\times2)p4g$ structures created by C and N adsorption on Ni(100) surfaces [Fig. 1(a)].[12,13] Here the adsorbate fills alternate fourfold hollow sites as in a $c(2\times2)$ structure ($\frac{1}{2}$-ML coverage). However, the presence of the adsorbate displaces the surface substrate atoms radially outward in the surface plane. To accommodate this radial expansion, the groups of four substrate atoms surrounding each adsorption site move tangentially in alternate clockwise and anticlockwise rotations. One possible reason why this reconstruction should occur at the same $\frac{1}{2}$-ML coverage as the $c(2\times2)$ phase is given by the SPA-LEED and STM study.[3] It is suggested the apparent disorder observed during the SPA-LEED measurements of the Rh(100)-$c(2\times2)$-O surface results from the formation of islands, the edges of which act to reduce the surface strain. Saturating the surface with further O atoms forces the islands to coalesce, and therefore an alternative means of reducing the surface stress is required. This is provided by the $(2\times2)p4g$ surface reconstruction.

Angle-resolved photoemission spectra along the $\Gamma X''$ direction [in the (2×2) Brillouin zone, see Fig. 1(b)] of the Rh(100)-$(2\times2)p4g$-O surface[11] show a strong photoemission feature centered between 4.4 and 5.8 eV. The study strong was performed at the Rh $4d$ Cooper minimum (photon energy 130 eV) and the dispersion of the feature was attributed to be solely the result of O $2p$ states. It was also found that the dispersion of the assigned O $2p$ peak only returns to the same energy at the center of even numbered

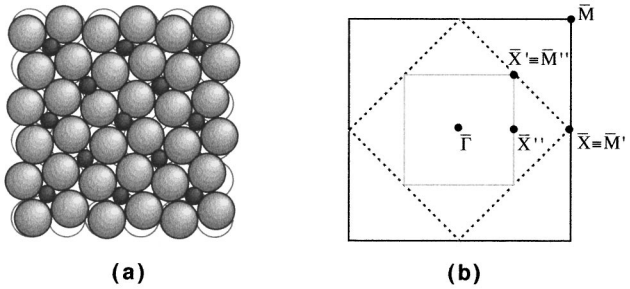

FIG. 1. (a) Real space model of $(2\times2)p4g$-O structure: large grey spheres indicate the surface Rh atoms, small dark spheres indicate the adsorbed O atoms. The empty circles show the positions of the Rh atoms prior to the reconstruction. (b) Brillouin zones: solid black line and unprimed symmetry points indicate the (1×1) zone, dashed black line and single primed symmetry points indicate the $c(2\times2)$ zone, and solid grey line and double primed symmetry points indicate the (2×2) zone.

(2×2) Brillouin zones. This apparent Brillouin zone doubling is expected for $(2\times2)p4g$ symmetry surfaces.[14,15] Additional measurements were also taken with the polarization vector of the incident light along the [010] direction, parallel to the surface and emission along the [001] direction, 6° from normal. In this geometry it was expected that only p_x and p_y states would be detected. Surprisingly, no oxygen-induced features were observed. It was suggested that this could be the result of empty p_x and p_y states or broadening due to strong hybridization with the metal surface. Therefore the O feature observed dispersing with a binding energy between 4.4 and 5.8 eV was tentatively assigned as a p_z state.[11] This is in contrast to an angle-resolved photoemission study[16] that shows that a feature assigned as p_z in character for the unreconstructed Ni(100)-$c(2\times2)$-O is apparently absent for both the reconstructed Ni(100)-$(2\times2)p4g$-C and Ni(100)-$(2\times2)p4g$-N surfaces. This is thought to be the result of stronger p_z-substrate hybridization for both $(2\times2)p4g$ surfaces, causing a broadening of the adsorbate p_z derived states. This was confirmed by a surface extended x-ray adsorption fine structure (SEXAFS) study of the Ni(100)-$c(2\times2)$-O and Ni(100)-$(2\times2)p4g$-N surfaces,[17] which suggested that the difference in bonding strength for C, N, and O demonstrated by the adsorbate-Ni bond length, is linked to the partial filling of the adsorbate $2p$ levels. The completely occupied O p_z orbital does not contribute to O-Ni bonding. Both C and N, which respectively have unoccupied or partially filled p_z orbitals, are more likely to form a bond with the second-layer Ni atoms and cause a $(2\times2)p4g$ reconstruction.

The surface structure of the S on Rh(100) system has been previously investigated using several techniques[4,8,18–21] including LEED,[18,19] high-resolution electron energy-loss spectroscopy,[3] normal incidence standing x-ray wave field adsorption (NISXW),[4] SEXAFS,[20] and self-consistent scattering theory.[21]

Experimentally it has been found that with increasing coverage, $p(2\times2)$ and $c(2\times2)$ phases are formed.[18,19] LEED intensity versus energy curves [LEED $I(E)$] and multiple scattering calculations[19] surprisingly suggested that for both phases the S atoms do not sit in symmetric fourfold hollow sites but are shifted between 0.27 and 0.28 Å away from the center of the fourfold hollow, towards bridge sites. However, recent NISXW measurements of the Rh(100)-$c(2\times2)$-S surface[4] indicate that this is not the case and as expected the most likely adsorption site is in the center of the fourfold hollow. Subsequent SEXAFS measurements[20] confirm this result, which is consistent with S adsorption on other fcc(100) surfaces.[4]

In this study angle-resolved photoemission spectra have been taken along the ⟨100⟩ ($\Gamma X'$) and ⟨110⟩ ($\Gamma M'$) principal azimuths for the Rh(100)-$c(2\times2)$-O, Rh(100)-$(2\times2)p4g$-O, and Rh(100)-$c(2\times2)$-S surfaces. In order to help with the interpretation of the experimental results, density of state (DOS) calculations for the Rh(100)-$c(2\times2)$-O and Rh(100)-$c(2\times2)$-S surfaces have also been performed.

II. EXPERIMENTAL DETAILS

The experiments were conducted on the IRC beamline 4.1 (Ref. 22) at the CLRC Daresbury Synchrotron Radiation Source. The beam line was equipped with a standard surface science ultrahigh vacuum (UHV) chamber (base pressure typically 2×10^{-10} mbar), incorporating LEED optics and a VSW HA54 hemispherical analyzer (0.5° angular resolution) mounted on a two-axis goniometer. From previous calibrations the estimated total energy resolution (photon energy and electron energy) at 38-eV photon energy is about 40 meV.[23]

The sample was prepared by repeated cycles of argon-ion bombardment, annealing between 1100 and 1200 K, annealing in oxygen, and reduction in hydrogen. The latter oxidation-reduction process effectively removes any surface contaminants, e.g., carbon and residual oxygen. The sample was deemed to be clean when the LEED showed a sharp (1×1) pattern and x-ray photoelectron spectroscopy (XPS) showed no significant amounts of contamination.

To prevent CO and H contamination from the residual gases in the UHV chamber, while taking angle-resolved measurements from the clean Rh(100) surface, the sample was flashed to 1200 K every set of four scans. Similar procedures have been adopted during other experimental studies of Rh surfaces.[24,25]

The two oxygen structures were prepared by background dosing the clean Rh(100) surface in front of the LEED optics. However O on Rh(100) surface structures can be removed by residual H or CO present in the chamber. As a result it was found that both the $c(2\times2)$-O and $(2\times2)p4g$-O LEED patterns deteriorated with time. Therefore during the course of each complete set of angle-resolved electron distribution curve (EDC) scans the $c(2\times2)$-O surface was reprepared several times. As the $(2\times2)p4g$-O phase occurs at saturation, the structure was maintained during the measurements by maintaining a continuous flow of 1×10^{-9} mbar of oxygen.

The Rh(100)-$c(2\times2)$-S surface was prepared by dosing the clean Rh(100) surface with H_2S while watching the LEED pattern. After a sharp $c(2\times2)$ pattern was formed the sample was then flashed to ~400 K to remove the H atoms, leaving strongly chemisorbed S on the surface.

The angle-resolved photoemission EDC scans were taken in the direction of the two principal azimuths, ⟨100⟩ and ⟨110⟩ [$\Gamma X'$ and $\Gamma M'$, respectively, in the $c(2\times2)$ Brillouin zone]. Preliminary measurements taken over a range of photon energies and emission angles showed that the best operating condition for subsequent measurements was at photon energy 38 eV. Angle-resolved measurements for all three overlayer structures were taken in the plane of incidence of the plane-polarized light, with an angle of incidence $\alpha=45°$ relative to the surface normal. This experimental geometry enables even parity states to be detected. During each set of scans the analyzer was moved in 2° steps.

III. CALCULATIONS

Local density of state (LDOS) calculations were performed using the BIOSYM electronic structure of close packed solids (ESOCS) package,[26] which utilizes the density-functional method previously described by Hohenberg and Kohn.[27–29]

The density of states were calculated for the clean Rh(100), Rh(100)-$c(2\times2)$-O, and Rh(100)-$c(2\times2)$-S sur-

faces. The unit cell for each calculation consisted of nine layers of Rh atoms, with each nine-layer slab separated by approximately 10 Å of vacuum (achieved by filling with empty spheres). Calculations using slabs larger than nine layers showed no appreciable differences to the nine-layer calculations but required more processor time. For adsorbate-covered surfaces the adsorbate atom was placed in the appropriate position on either side of the Rh slab. The distance between the O atoms and the surface plane was obtained from a LEED $I(E)$ study of the Rh(100)-$p(2\times2)$-O surface ($d_{01}=0.95$ Å).[9] Similarly, the distance between the S atoms and the surface plane was obtained from a NISXW study of the Rh(100)-$c(2\times2)$-S surface ($d_{01}=1.38$ Å).[4]

Full calculations were not performed for the Rh(100)-$(2\times2)p4g$-O structure due to the increased size of the unit cell and the associated increase in processing time. However, preliminary calculations for the $(2\times2)p4g$-O surface using a three-layer Rh slab showed no significant differences from the $c(2\times2)$-O calculation.

IV. RESULTS AND DISCUSSION

A. Assignment of features

We now discuss the assignment of features in the photoemission spectra. DOS calculations are useful in the understanding of the nature of the adsorbate-substrate bond and we use them here as a guide to identification and assignment of the peaks. However, we acknowledge that matrix element effects (selection rules and cross-sectional variations) mean that a direct comparison of DOS calculations with photoemission spectra is not possible. Hence we do not rely solely on the DOS calculations but also draw on comparisons between the spectra from the clean and adsorbate-covered surfaces and on previously published work on the O on Rh(100) system.[11]

Figure 2 shows the results of the total LDOS calculations for the surface Rh atoms and where appropriate the adsorbate atoms, for the clean Rh(100), Rh(100)-$c(2\times2)$-O and Rh(100)-$c(2\times2)$-S surfaces. From the analysis of the projected DOS (not shown) the total surface Rh LDOS for each surface structure are largely dominated by Rh d states, while the total adsorbate LDOS are predominantly the result of adsorbate p states. The total O LDOS [Fig. 2(b)] shows a broad peak between binding energies of 4 and 6.4 eV, while the total S LDOS [Fig. 2(c)] only shows a gradual increase between 2 and 6.4 eV. For both the $c(2\times2)$-O and $c(2\times2)$-S surfaces the presence of the adsorbate causes a slight drop in the surface Rh LDOS between binding energies of 3 and 4 eV and an increase in the LDOS at 6 eV, demonstrating a shift of the antibonding states towards higher energies. The adsorbate-covered surfaces also show a relative increase in the unoccupied states above the Fermi level. Both of these effects are indicative of adsorbate-surface hybridization.

The angle-resolved spectra for the Rh(100)-$c(2\times2)$-O, Rh(100)-$(2\times2)p4g$-O, and Rh(100)-$c(2\times2)$-S surfaces are plotted in Figs. 3, 4, and 5, respectively. Each scan has been normalized to the background (at a binding energy of ~9 eV), and plotted with the normalized clean Rh(100) surface scan taken at the same emission angle. Comparison of the clean and dosed spectra clearly reveals significant differences both near the Fermi edge and in the adsorbate p-state

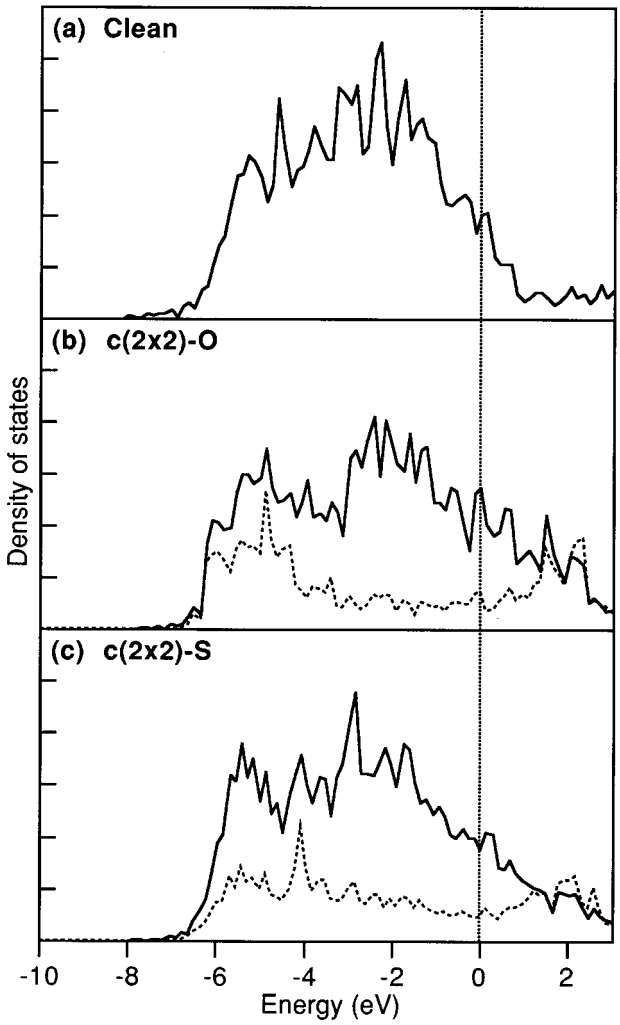

FIG. 2. Calculated local density of states (LDOS) for (a) clean Rh(100), (b) Rh(100)-$c(2\times2)$-O, and (c) Rh(100)-$c(2\times2)$-S. In each case solid curves indicate total surface Rh LDOS and dotted curves show the total adsorbate LDOS.

peak energy region (between 3 and 6 eV). The very high intensity of the Rh states just below the Fermi level (between 0 and 3 eV) makes it difficult to distinguish adsorbate-induced states in this region. Therefore we confine our discussion to the features in the 3–6-eV region. In this region adsorbate-induced features can be clearly identified (see Figs. 3–5). This is the region where the adsorbate-related changes in the spectra are expected, according to the LDOS calculations. Both the O- and S-induced states are broad with a width of the order 1.5–2 eV and this is in good agreement with the LDOS calculations.

The binding energy of each feature that shows a significant difference in behavior (change in position or intensity) from features observed on the corresponding clean Rh(100) EDC scans, between a binding energy of 3 and 6 eV, has been plotted against parallel momentum $\mathbf{k}_{\|}$ for the $c(2\times2)$-O [Fig. 6(a)], $(2\times2)p4g$-O [Fig. 6(b)], and $c(2\times2)$-S [Fig. 6(c)] surfaces. The dispersion of these states is also shown on Figs. 3–5. Any gaps in the bandmap plots indicate regions where the new features could not be clearly resolved from the clean Rh(100) peaks.

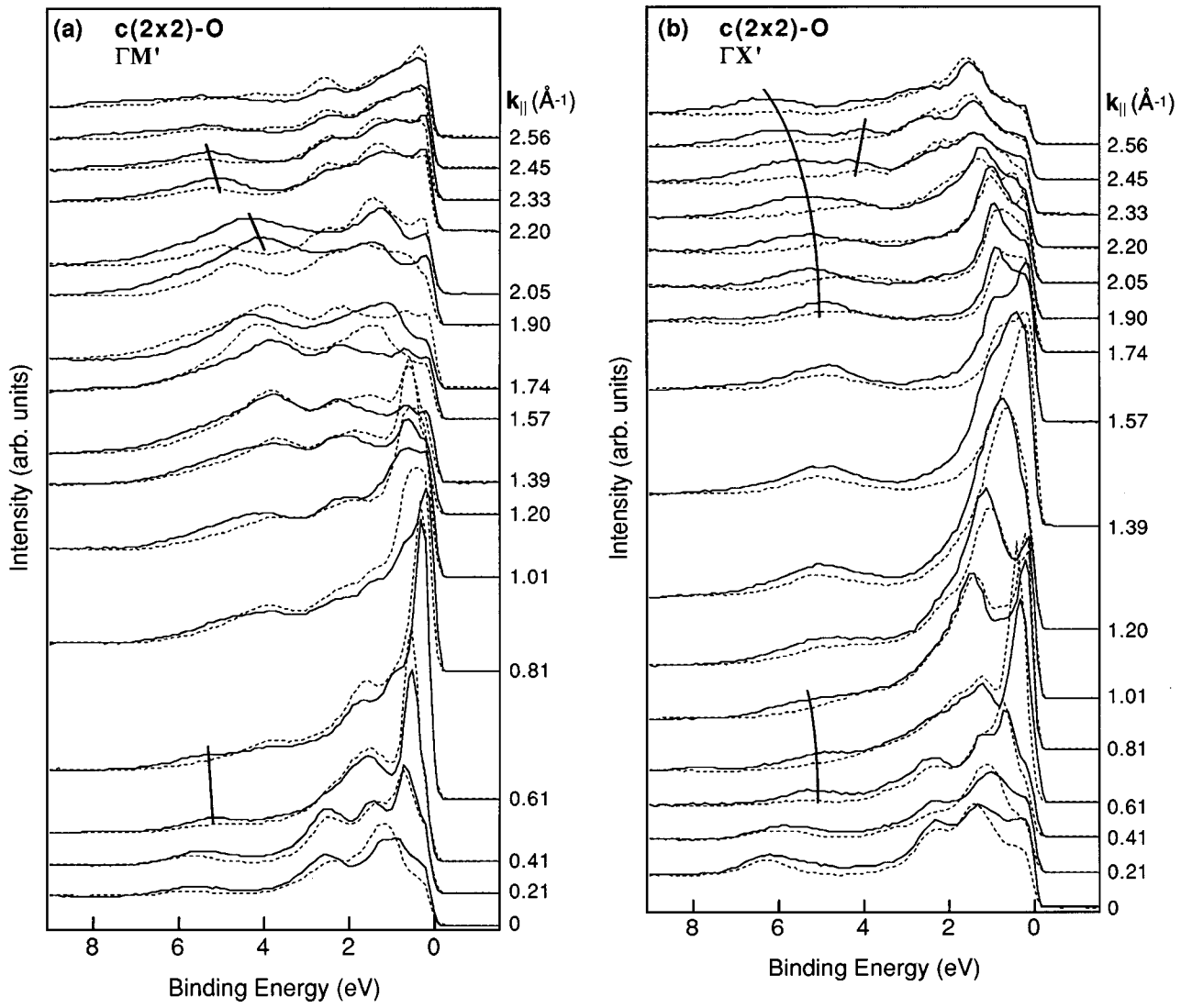

FIG. 3. Angle-resolved photoemission spectra shown in 4° steps, from the clean Rh(100) (dotted curves) and Rh(100)-$c(2\times2)$-O (solid curves) surfaces. Scans were taken at a photon energy of 38 eV. The parallel momenta $\mathbf{k}_{\parallel}$ shown are calculated for electrons emitted from the Fermi level. The lines between adjacent spectra indicate the dispersion of clearly resolvable features due to O adsorption. (a) shows data collected along $\Gamma M'$ direction; (b) shows data collected along $\Gamma X'$ direction.

The data have been represented in the reduced zone scheme by back folding into the $c(2\times2)$ Brillouin zone (Fig. 7). The $(2\times2)p4g$-O bands are not back folded into the expected (2×2) Brillouin zone because of the possible occurrence of apparent zone doubling.[14,15] As mentioned in the Introduction a previous angle-resolved study of the Rh(100)-$(2\times2)p4g$-O surface,[11] showing the dispersion of the O $2p$ peak along the $\langle 110\rangle$ direction, demonstrated the effect of apparent zone doubling. This effect is related to the existence of glide symmetry lines.[14] Our results from the Rh(100)-$(2\times2)p4g$-O surface taken along the same $\langle 110\rangle$ direction and plotted in the extended (2×2) zone scheme (Fig. 7) show a similar behaviour, i.e., the dispersion only returns to the same energy at the center of even-numbered (2×2) Brillouin zones. This graphically illustrates why the data presented in Fig. 6 have been folded into the $c(2\times2)$ Brillouin zone. However, it should be noted that this effect may not necessarily be due to the presence of the glide symmetry lines in the topmost layers of the surface. McConville *et al.*[30] have pointed out that it may be the dominance of the adsorbate periodicity with respect to the bulk substrate that determines the Brillouin zone size.

B. Differences in the $c(2\times2)$-O and $(2\times2)p4g$-O results

The dispersion of the even parity bands centered between 4 and 6 eV for both the $c(2\times2)$-O [Fig. 6(a)] and $(2\times2)p4g$-O [Fig. 6(b)] surfaces show several differences. Along the $\Gamma X'$ direction of the $c(2\times2)$-O structure, points from the first and second Brillouin zones show a similar dispersion to that observed for the $(2\times2)p4g$-O phase. Points taken from the third zone show two new bands, one dispersing upwards towards 4 eV and one dispersing downward to 6 eV. The intensity of these features is greater outside the first and second Brillouin zones; such effects have been previously documented.[16,31] Along the $\Gamma M'$ direction

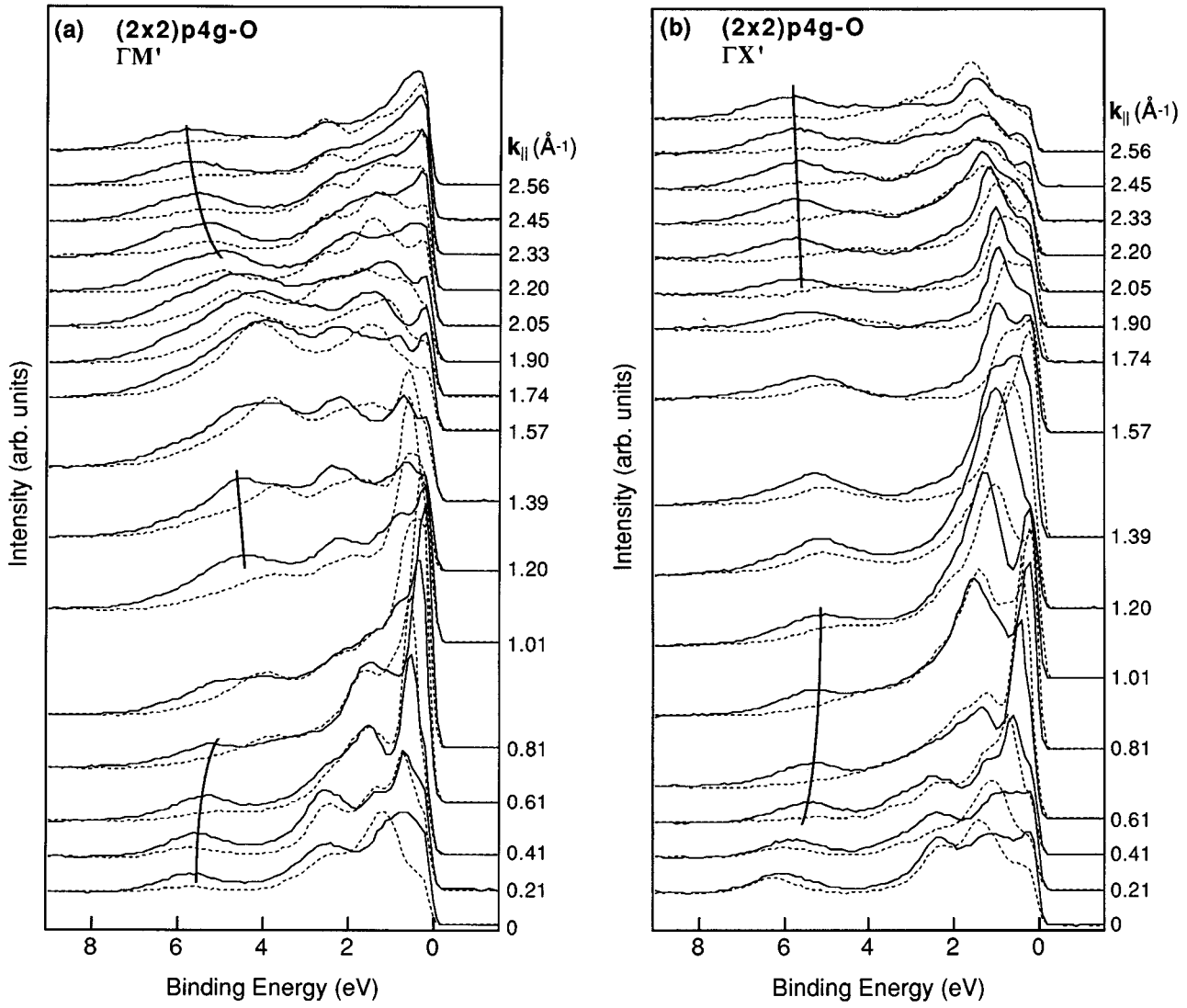

FIG. 4. Angle-resolved photoemission spectra shown in 4° steps, from the clean Rh(100) (dotted curves) and Rh(100)-(2×2)$p4g$-O (solid curves) surfaces. Scans were taken at a photon energy of 38 eV. The parallel momenta $\mathbf{k}_{\parallel}$ shown are calculated for electrons emitted from the Fermi level. The lines between adjacent spectra indicate the dispersion of clearly resolvable features due to O adsorption. (a) shows data collected along $\Gamma M'$ direction; (b) shows data collected along $\Gamma X'$ direction.

the $c(2\times2)$-O band also splits upwards towards 4 eV and downwards towards 6 eV. Again the splitting is only seen from points folded from higher Brillouin zones. This is in contrast to the (2×2)$p4g$-O bands where data points folded from higher zones in both the $\Gamma M'$ and $\Gamma X'$ directions are consistent with points taken from the first zone. The dispersions observed for both the $c(2\times2)$-O and (2×2)$p4g$-O structures are quite large (>1 eV) and suggest a large overlap of atom wave functions.

We now discuss the relation between these differences in electronic structure and the different geometries of the two systems. Previous angle-resolved photoemission work comparing the experimentally determined bands from the Ni(100)-$c(2\times2)$-O surface with the Ni(100)-$p4g$-N and Ni(100)-$p4g$-C structures also show significant differences between the (2×2)$p4g$ and $c(2\times2)$ band structures.[16] It was argued that the fact that the N and C atoms are coplanar (see Refs. 32 and 33) with the top layer Ni atoms is likely to have a profound effect on the dispersions. A coplanar geometry allows a stronger adsorbate-to-metal interaction and in particular a stronger interaction with the second-layer metal atoms. However, it is not clear this is the case for Rh(100). To our knowledge there are no experimental data available that show the O-Rh interlayer spacing for the Rh(100)-(2×2)$p4g$-O surface is significantly smaller than that for the Rh(100)-$c(2\times2)$-O surface. In fact it has been speculated from previous SPA-LEED and STM measurements that even for the $c(2\times2)$-O surface the O may sit in an expanded hollow, similar to the (2×2)$p4g$-O structure. If this is the case then the observed differences in dispersion of the O-induced bands are likely to be a result of the (2×2)$p4g$ reconstruction, i.e., the twisting of the topmost Rh atoms.

Finally we turn to differences in the band structures between the Rh(100)-(2×2)$p4g$-O system and the Ni(100)-(2×2)$p4g$-C and Ni(100)-(2×2)$p4g$-N systems.

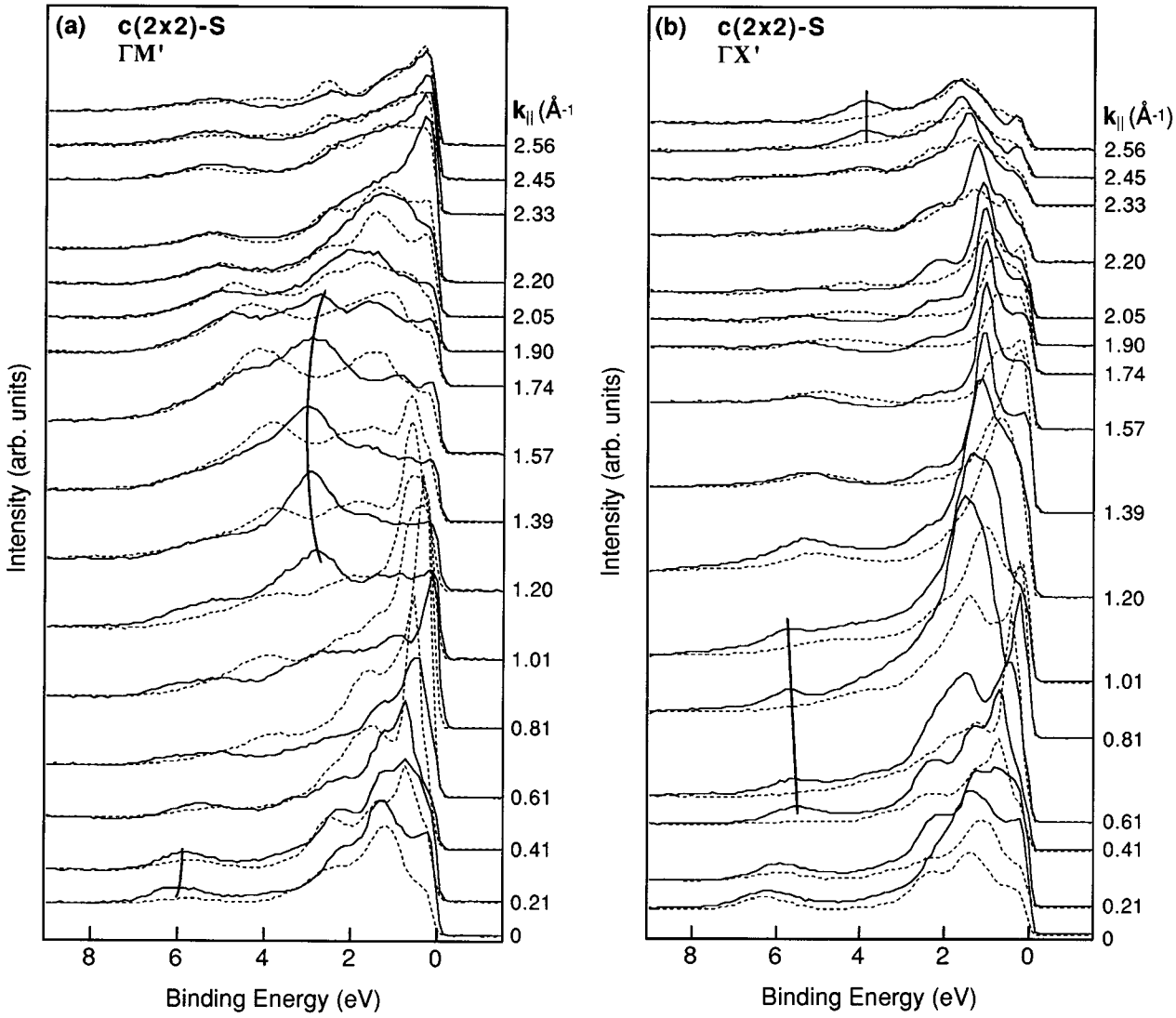

FIG. 5. Angle-resolved photoemission spectra shown in 4° steps, from the clean Rh(100) (dotted curves) and Rh(100)-$c(2\times2)$-S (solid curves) surfaces. Scans were taken at a photon energy of 38 eV. The parallel momenta $\mathbf{k}_{\parallel}$ shown are calculated for electrons emitted from the Fermi level. The lines between adjacent spectra indicate the dispersion of clearly resolvable features due to S adsorption. (a) shows data collected along $\Gamma M'$ direction; (b) shows data collected along $\Gamma X'$ direction.

The Ni(100) angle-resolved photoemission study[16] shows that between 4 and 7 eV both the $(2\times2)p4g$-C and $(2\times2)p4g$-N bands disperse downwards, which is in contrast to our results for the Rh(100)-$(2\times2)p4g$-O surface [Fig. 6(b)], which show an upward dispersion of the $(2\times2)p4g$-O bands over the same energy range. However, the adsorption of O does not reconstruct the Ni(100) surface and there are also marked differences between the Rh and Ni valence-band structure. For the Ni(100)-$c(2\times2)$-O surface, electronic structure calculations have shown that the adsorbate $2p$ states hybridize with the substrate $3d$ and $4sp$ states.[34] As demonstrated by our DOS calculations for the Rh(100)-$c(2\times2)$-O surface, the adsorbate $2p$ states hybridize with Rh $4d$ states. This may explain the differences between the dispersions of adsorbate-induced bands on Rh(100) and Ni(100) surfaces.

C. The Rh(100)-$c(2\times2)$-S system

Figure 6(c) shows the dispersion of the Rh(100)-$c(2\times2)$-S even parity bands. The band at approximately 4 eV near the X' point shows a similar behavior to that observed on the $c(2\times2)$-O surface, indeed both bands result from back folding from higher zones. This band is not observed for the $(2\times2)p4g$-O system and this absence may reflect the geometry of the $(2\times2)p4g$ reconstruction itself.

A clearly resolved band can be seen dispersing between 5 and 6.2 eV along the whole length of the Brillouin zone, in both the $\Gamma M'$ and $\Gamma X'$ directions. This band shows marked differences to the bands observed for the $c(2\times2)$-O and $(2\times2)p4g$-O surfaces, especially near the Γ point. The band at approximately 3 eV shows very little dispersion but is of interest as no similar features are seen on the clean or O dosed Rh surfaces. Inspection of Fig. 5(a) shows the inten-

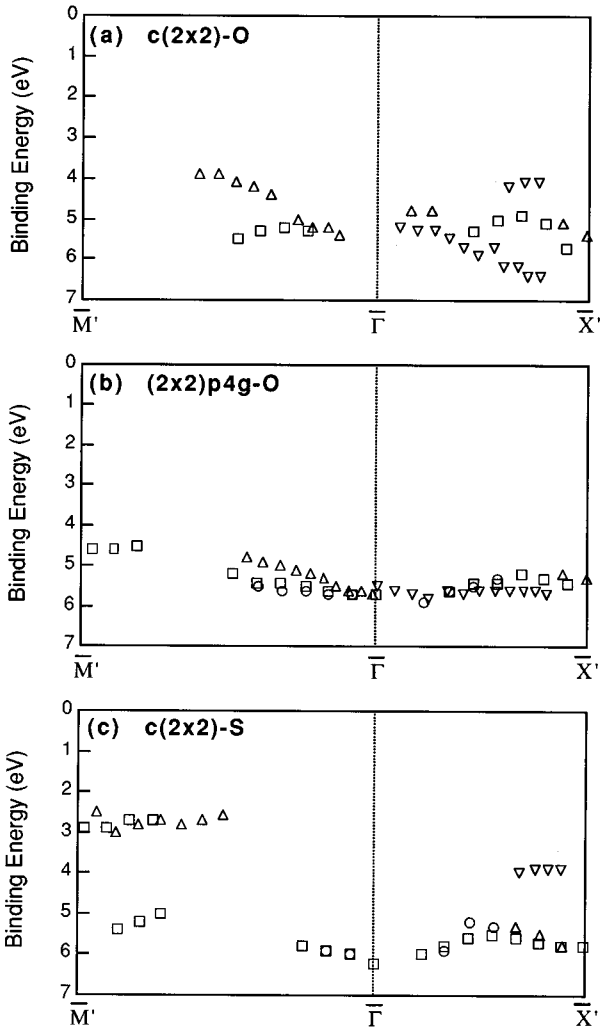

FIG. 6. Experimentally determined bands derived from features that show significant differences to clean Rh features, the binding energy of each feature is plotted against the corresponding parallel momentum $\mathbf{k}_{\|}$ in the reduced zone scheme. Measurements were taken in the plane of incident radiation and therefore show even states. ○ indicate data points from the first negative Brillouin zone, □ indicate data points from the first zone, △ indicate data points from the second zone, and ▽ indicate data points from the third zone.

sity of this feature dominates at $\mathbf{k}_{\|}$ values between 1.2 and 2.2 Å^{-1}. As the LDOS calculations show no significant S features in this energy region, such changes could be the result of S-Rh hybridized states.

The differences in dispersion between the $c(2\times2)$-S band and the O-induced band for both the $c(2\times2)$-O and $(2\times2)p4g$-O surfaces at 5–6 eV may be a result of the larger atomic radius of the S atom. Sander, Linke, and Ibach[35] measured the surface stress induced by the adsorption of C, O, and S on the Ni(100) surface as a function of the adsorbate coverage and obtained good agreement with theory for the lighter atoms, but deviations for S. These deviations were ascribed to the fact that adsorbate-adsorbate interactions were neglected in their model clusters; i.e., the increased size of the S atomic radius compared to the O may modify the

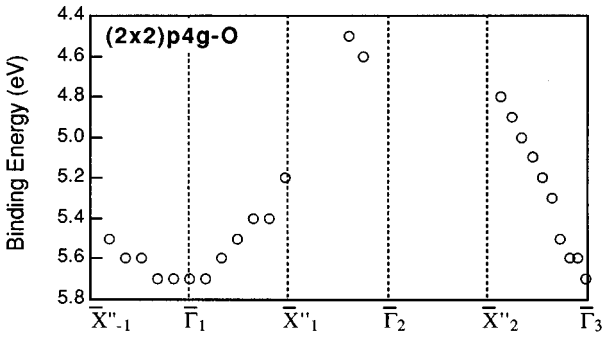

FIG. 7. Experimentally determined Rh(100)-$(2\times2)p4g$-O bands plotted in the (2×2) extended zone scheme to show the effect of apparent band doubling.

balance between the adsorbate-adsorbate and adsorbate-substrate interactions. Presumably this may also be reflected in the band structure.

V. CONCLUSIONS

We have calculated the LDOS for the clean Rh(100), Rh(100)-$c(2\times2)$-O, and Rh(100)-$c(2\times2)$-S surfaces. Comparisons between the LDOS of the clean and adsorbate-covered Rh(100) surfaces reveal subtle changes in the surface Rh d states between 4 and 6 eV and just above the Fermi level, suggesting substrate-adsorbate hybridization. The LDOS calculations also show that states localized at the adsorbate atoms are mainly $2p$ in character. Comparison between the angle-resolved photoemission spectra for each overlayer structure and the corresponding clean Rh(100) spectra clearly show the presence of adsorbate-induced features between 3 and 6 eV binding energy, which we deduce have predominantly adsorbate p-state character.

The dispersion of these features for the $c(2\times2)$-O, $(2\times2)p4g$-O, and $c(2\times2)$-S surfaces show distinct differences. The observed differences between the dispersion of the O-derived states for the $c(2\times2)$-O and $(2\times2)p4g$-O surfaces demonstrate that the distortion of the topmost Rh layer may have a greater effect on the band structure than that previously proposed for the related Ni(100)-$(2\times2)p4g$-C/N systems in Refs. 16 and 30. The dispersion of the S states for the $c(2\times2)$-S surface show two distinct bands that remain split throughout the Brillouin zone. We tentatively attribute the low binding energy band to adsorbate-induced states with some Rh $4d$ character. There are greater similarities to the $c(2\times2)$-O structure rather than the $(2\times2)p4g$-O structure, suggesting again that the $(2\times2)p4g$ structure does influence the band structure; however, the different behaviour of the S and O bands may also be influenced by the differences in atomic radii.

ACKNOWLEDGMENTS

The authors would like to thank EPSRC for financial support, and CLRC Daresbury Laboratory for access to the SRS and for providing support for J.R.M. We thank S. D. Barrett for helpful discussions and P. L. Wincott for a critical reading of the manuscript. We would also like to thank Sincrotrone Trieste for the loan of the Rh(100) sample.

*Present address: Department of Physics, Universite Joseph Fourier, Grenoble, France.

†Author to whom correspondence should be addressed. Also at Department of Physics, The University of Liverpool, P.O. Box 147, Liverpool L69 3BX, United Kingdom. Electronic address: mcgrath@ssci.liv.ac.uk

[1] A. Bielanski and J. Haber, *Oxygen in Catalysis* (Dekker, New York, 1991).

[2] M. P. Kiskinova, Surf. Sci. Rep. **8**, 359 (1988).

[3] J. R. Mercer, P. Finetti, F. M. Leibsle, R. McGrath, V. R. Dhanak, A. Baraldi, K. C. Prince, and R. Rosei, Surf. Sci. **352–354**, 173 (1996).

[4] J. R. Mercer, G. Scarel, A. Santoni, B. C. C. Cowie, D. Lewis, A. W. Robinson, R. McGrath, and V. R. Dhanak, Surf. Sci. **369**, 36 (1996).

[5] C. W. Tucker, J. Appl. Phys. **37**, 3013 (1966).

[6] D. G. Castner, B. A. Sexton, and G. A. Somorjai, Surf. Sci. **71**, 519 (1978).

[7] W. H. Daniel, Y. Kim, H. C. Peebles, and J. M. White, Surf. Sci. **111**, 189 (1981).

[8] L. H. Dubois, J. Chem. Phys. **77**, 5228 (1982).

[9] W. Oed, B. Dötsch, L. Hammer, K. Heinz, and K. Müller, Surf. Sci. **207**, 55 (1988).

[10] A. Baraldi, V. R. Dhanak, G. Comelli, K. C. Prince, and R. Rosei, Phys. Rev. B **53**, 4073 (1996).

[11] M. Zacchigna, C. Astaldi, K. C. Prince, M. Sastry, C. Comicioli, R. Rosei, C. Quaresima, C. Ottaviani, C. Crotti, A. Antonini, M. Matteucci, and P. Perfetti, Surf. Sci. **347**, 53 (1996).

[12] J. H. Onuferko, D. P. Woodruff, and B. W. Holland, Surf. Sci. **87**, 357 (1979).

[13] W. Daum, S. Lehwald, and H. Ibach, Surf. Sci. **178**, 528 (1996).

[14] K. C. Prince, M. Surman, Th. Linder, and A. M. Bradshaw, Solid State Commun. **59**, 71 (1986).

[15] K. C. Prince, J. Electron. Spectrosc. Relat. Phenom. **42**, 217 (1987).

[16] A. L. D. Kilcoyne, D. P. Woodruff, J. E. Rowe, and R. H. Gaylord, Phys. Rev. B **39**, 12 604 (1989).

[17] L. Wenzel, D. Arvanitis, W. Daum, H. H. Rothermund, J. Stöhr, K. Baberschke, and H. Ibach, Phys. Rev. B **36**, 7689 (1987).

[18] S. Hengrasmee, P. R. Watson, D. C. Frost, and K. A. R. Mitchell, Surf. Sci. **87**, L249 (1979).

[19] W. Liu, J. R. Lou, and K. A. R. Mitchell, Surf. Sci. **281**, 21 (1993).

[20] V. R. Dhanak, S. P. Harte, G. Scarel, B. C. C. Cowie, and A. Santoni, Surf. Sci. Lett. **366**, L765 (1996).

[21] P. J. Feibelman, Phys. Rev. B **43**, 9452 (1991).

[22] V. R. Dhanak, A. W. Robinson, G. van der Laan, and G. Thornton, Rev. Sci. Instrum. **63**, 1342 (1992).

[23] V. R. Dhanak (private communication).

[24] W. Di, S. Dhar, K. E. Smith, and S. D. Kevan, Phys. Rev. B **49**, 4821 (1994).

[25] S. C. Wu, K. Garrison, A. M. Begley, F. Jona, and P. D. Johnson, Phys. Rev. B **49**, 14 081 (1994).

[26] BIOSYM/MSI, 9685 Scranton Road, San Diego, CA 92121-3752.

[27] P. Hohenberg and W. Kohn, Phys Rev. **136**, B864 (1964).

[28] J. Kuebler and V. Eyert, *Electronic and Magnetic Properties of Metals and Ceramics*, Materials Science and Technologies Series Vol. 3A (VCH Verlagsgesellschaft, Weinheim, 1991), pp. 1–145.

[29] R. O. Jones and O. Gunnarsson, Rev. Mod. Phys. **61**, 689 (1989).

[30] C. F. McConville, D. P. Woodruff, S. D. Kevan, M. Weinert, and J. W. Davenport, Phys. Rev. B **34**, 2199 (1986).

[31] S. Y. Tong, C. H. Li, and A. R. Lubinsky, Phys. Rev. Lett. **39**, 498 (1977).

[32] A. L. D. Kilcoyne, D. P. Woodruff, A. W. Robinson, Th. Linder, J. S. Somers, and A. M. Bradshaw, Surf. Sci. **253**, 107 (1991).

[33] Y. Gauthier, R. Baudoing-Savois, K. Heinz, and H. Landskron, Surf. Sci. **251/252**, 493 (1991).

[34] A. Liebsch, Phys. Rev. B **17**, 1653 (1978).

[35] D. Sander, U. Linke, and H. Ibach, Surf. Sci. **272**, 318 (1992).